Clay Minerals, (2013) **48**, 391–402

Micro-scale experimental investigation of the swelling anisotropy of the Callovo-Oxfordian argillaceous rock

L. L. WANG[1,*], M. BORNERT[2], S. CHANCHOLE[1], D. S. YANG[3], E. HÉRIPRÉ[1], A. TANGUY[1] AND D. CALDEMAISON[1]

[1] *Laboratoire de Mécanique des Solides (UMR 7649), École Polytechnique, 91128 Palaiseau Cedex, France,* [2] *Laboratoire Navier (UMR 8205), CNRS, ENPC, IFSTTAR, Université Paris-Est, 77455 Marne-la-Vallée Cedex, France, and* [3] *State Laboratory of Geomechanics and Geotechnical Engineering, IRSM, Chinese Academy of Science, 430071 Wuhan, China*

(*Received 4 December 2012; revised 19 March 2013; Editor: John Adams*)

ABSTRACT: An experimental study of the swelling anisotropy of the Callovo-Oxfordian argillaceous rock under hydration is presented. The investigation, which combines environmental scanning electron microscopy (ESEM) and digital image correlation techniques, has been carried out at the micrometric scale of the composite microstructure of the rock. Specimens were hydrated in the ESEM over a wide range of relative humidity and observations conducted on two planes: plane 1 parallel to the bedding plane, and plane 2 perpendicular to it. The observations reveal that the local swelling (which can be quantified at a local gauge length of about 5 μm) is strongly anisotropic in both planes. The global swelling, measured over areas of about 500 μm in width, is also clearly anisotropic in plane 2 (with major swelling direction normal to the bedding plane), but not in plane 1. The global isotropy in plane 1 arises from the uniform distribution of the orientation of anisotropic local strains, while the anisotropic swelling in plane 2 is due to a preferred local orientation.

KEYWORDS: argillaceous rocks, radioactive waste repository, anisotropic swelling, environmental scanning electron microscopy, digital image correlation, local strain field, geomechanics.

The Callovo-Oxfordian (COx) argillaceous rock is being studied as a potential host rock for an underground radioactive waste repository in France, because of its low permeability and other favourable properties. A key feature of this material is its swelling property (i.e. considerable volume increase under wetting), essentially induced by the clay minerals it contains. The swelling of COx argillaceous rock has been found to be anisotropic on the macro-scale: it is much more significant along the direction perpendicular to the bedding plane than along the directions parallel to it (Pham *et al.*, 2007; Valès, 2008; Yang *et al.*, 2012). This anisotropy can possibly be linked to various mechanisms, among which are: (1) preferred orientation of clay particles exhibiting anisotropic swelling and mechanical properties, (2) anisotropic shape, orientation and spatial distribution of other mineral inclusions, and (3) anisotropic micro-cracking induced by wetting. It is acknowledged that the clay particles play a key role in the swelling anisotropy of the argillaceous rock, essentially because of their layered microstructure. Indeed, swelling of clay particles is essentially an increase of inter-layer and inter-particle spaces, so that it is predominant along the direction perpendicular to the layers.

* E-mail: wang@lms.polytechnique.fr
DOI: 10.1180/claymin.2013.048.2.17

Anisotropy also exists for the mechanical properties of clay particles: the stiffness along the direction normal to the layers is much lower than along other directions (Sayers, 1994; Ortega *et al.*, 2007). Hence, the orientation of clay particles is a crucial parameter for swelling anisotropy. It sounds reasonable that the clay particles in this sedimentary rock are oriented such that the layers are preferentially parallel to the bedding plane. However, this is only partly confirmed by X-ray diffraction characterization, which reveals that the COx argillaceous rock shows a relatively weak alignment of clay minerals compared to other rocks (Wenk *et al.*, 2008). The other mineral inclusions (mostly carbonate and quartz) are insensitive to water and their mechanical properties can be considered to be more isotropic. However, their shape, orientation and spatial distribution might give rise to the swelling anisotropy through the mechanical interactions between these inclusions and clay. Indeed Valès (2008) has observed some anisotropy in the spatial distribution of the constitutive phases of this rock: larger calcite and quartz grains (above 150 μm in size) exhibiting an anisotropic shape are, for instance, preferentially oriented along the bedding plane; a similar preferred orientation is also observed for elongated clusters of smaller grains, as well as for pyrite veins. In addition, Wang (2012) has found evidence of a network of micro-cracks induced by wetting (with typical openings ~1 μm), preferentially extending parallel to the bedding plane. This anisotropic micro-cracking, which cannot be observed by unaided eyes, may also contribute to the anisotropy of the swelling strain recorded in the existing macroscopic experimental results.

Although the swelling anisotropy of the COx argillaceous rock has been confirmed on the macroscale, its microscopic mechanisms are still uncertain. In particular, the relative contribution of the various possible mechanisms mentioned above has not been evaluated. The purpose of this paper is to quantify the swelling of this rock at the particle scale and to characterize the spatial distribution of these swelling strains within the microstructure. The results provide an improved insight into the mechanisms of the swelling anisotropy.

MATERIAL

The tested material is the COx argillaceous rock from the Meuse/Haute-Marne underground research laboratory at Bure, in France. It contains 25−55% clay minerals (by weight), 23−42% carbonate (calcite, dolomite and ankerite), 20−31% quartz and feldspars, and a small percentage of subordinate minerals (ANDRA, 2005). The clay minerals in this rock are principally interstratified illite/smectite (I-S), illite, mica, chlorite and kaolinite, among which I-S is the most abundant.

The microstructure of argillaceous rocks has been extensively studied (Sammartino *et al.*, 2003; Robinet *et al.*, 2012). In general, such rocks appear as a composite made of a continuous clay matrix with mineral inclusions scattered. The size of quartz grains varies from 10 to 100 μm, while that of carbonate is more variable: micron-sized small grains are found together with larger particles which can reach 200 μm or more in length. Both carbonate and quartz grains, exhibiting statistically a moderately elongated shape, seem to be preferentially oriented parallel to the bedding plane (Valès, 2008; Robinet *et al.*, 2012). The 3D connectivity between other mineral particles and carbonate grains in particular however remains unclear.

EXPERIMENTAL METHOD

ESEM

The experimental investigation of this work benefited from a combination of high-resolution imaging with an environmental scanning electron microscope (ESEM) and digital image correlation (DIC) techniques. A series of "multi-step" wetting experiments and associated micro-scale observations were performed in an ESEM (FEI Quanta 600). The principle of controlling the relative humidity (RH) in the ESEM is as follows. By definition, the RH depends merely on temperature and water vapour pressure. The specimen temperature is controlled by a Peltier module which can be fitted on the ESEM motorized stage. The module used in this work enables temperatures in the range −20º to 50ºC to be obtained. By an iterative purge process, the dry air initially present in the ESEM chamber can be pumped out so that the chamber can be filled with water vapour only. Hence, wetting (increase of RH) can be achieved by controlling both the specimen temperature and the gas pressure, equal to the water vapour pressure, in the ESEM chamber.

In addition, a micro-scale observation by ESEM in back-scattered electron (BSE) mode reveals the

https://doi.org/10.1180/claymin.2013.048.2.17 Published online by Cambridge University Press

composite microstructure of this rock. The large inclusions appear as isolated domains with an almost uniform grey level (quartz grains are darker than calcites), while the clay matrix exhibits a micrometric heterogeneity. The presence of water vapour would degrade the image quality because it disturbs not only incident electrons but also the emitted signals. Since water vapour pressure increases with temperature for a given RH, it is desirable to keep the temperature as low as possible from the viewpoint of high image quality (i.e. highly contrasted images with as low as possible image noise) which is a key issue for DIC analysis. In this study, the RH is controlled by changing the ESEM chamber pressure at a constant temperature of 2ºC. We refer to Wang (2012) for a detailed discussion on this choice.

Strain field evaluation by DIC techniques

The images recorded by the ESEM were analysed by DIC techniques, which quantify local strain fields of the material. Generally speaking, the 2D-DIC technique permits measurement of in-plane components of the displacement field in observed zones with sub-pixel accuracy by searching matching-subsets between an image of some chosen reference configuration of the sample and images of the same area after deformation (Sutton *et al.*, 2009; Bornert *et al.*, 2011).

The in-house software CMV developed at the LMS and Navier laboratories, implementing the DIC method and various post-processing routines adapted to a micromechanical analysis (see Allais *et al.*, 1994, for details), is used for the DIC analysis and strain measurements performed here. Based on this analysis, the in-plane components of local strains (ε_{xx}, ε_{yy}, ε_{xy}) can be evaluated at some local gauge length depending on the image characteristics and chosen DIC parameters. In addition, the two in-plane eigenvalues of the 2D Green-Lagrange strain tensor (namely ε_1 and ε_2 with $\varepsilon_2 > \varepsilon_1$) and the angle θ between the ε_2 direction and the vertical axis of the reference image can be determined. These quantities can also be evaluated for the whole region of interest (ROI), and will be referred to by capital letters; for instance, global principal strains are E_1 and E_2. It is emphasized that the components of the deformation gradient relative to the whole ROI are by definition the spatial averages of the local ones, but E_1 is not the average of ε_1 because of possible local fluctuations of the angle θ.

The 2D observations in this work were performed on selected zones of the sample surface with a size of 256 μm × 221 μm (corresponding to a nominal SEM image magnification ×500), and the related images were recorded with high definition (4096 × 3536 pixels) for the DIC analysis. Hence, the physical length represented by a pixel is 62.5 nm. The matching-subset was chosen to be 40 × 40 pixels, i.e. 2.5 μm in physical size. According to this size and the procedure employed to compute local strains (making use of the displacements of the eight closest neighbouring positions of a given measurement position), the gauge length for local strain measurement is 80 × 80 pixels, i.e. 5 μm in real space. Under these experimental conditions, the standard deviation of the experimental errors in the measured local strain components in the clay matrix is about 0.1%, with the maximum below 1%. This error is larger in other mineral inclusions due to the lack of an appropriate local image contrast, but this is not really a problem since such inclusions do not swell.

Sample preparation and experimental procedure

To study the swelling anisotropy of the COx argillaceous rock, two observation planes were prepared on two separate samples extracted from the same core: plane 1 parallel to the bedding plane and plane 2 normal to it (see Fig. 1). Sheet-like

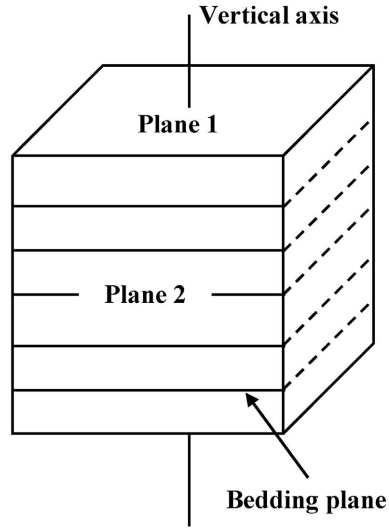

FIG. 1. Two observation planes.

https://doi.org/10.1180/claymin.2013.048.2.17 Published online by Cambridge University Press

specimens, with ~1 mm thickness and in-plane extensions of several millimetres, were prepared under standard room conditions. The small thickness can considerably reduce the time taken to reach the steady state after each wetting step for such a weakly permeable material. To obtain a smooth and well contrasted surface, specimens were polished with abrasive paper in four stages with an increasing grade from 800 to 4000. Moreover, special attention was paid to keeping both sides of the specimen flat and parallel so that the observation plane was perpendicular to the ESEM optical axis.

Both samples (one for each observation plane) were subjected to the same "multi-step" wetting test. At first they were cooled down to a temperature of 2ºC and the pressure was adjusted (249 Pa) so as to reach a RH of 35%. Its steady state serves as reference configuration for strain measurements. Four subsequent RH steps were then obtained (Fig. 2) by adjusting the chamber vapour pressure while keeping the temperature constant. In the last step, the pressure was 713 Pa corresponding to a very high RH of 99%. Specimens were unconfined during the test (i.e. free swelling condition). For each wetting step, the RH was modified at a fixed rate (5% RH/min) until the prescribed value was reached. This moderate rate of RH change rate helps to avoid micro-cracking at high RH levels which has been observed at higher rates (Wang, 2012). Then the ESEM chamber pressure was maintained constant until the steady state for the given RH was reached. BSE images of eight ROIs (four for each observation plane) selected for the DIC analysis were recorded every 30 minutes during this transient moisture transport stage. Moisture equilibrium was considered to be reached once the overall incremental strain measured between two images recorded successively was sufficiently small for all these observation zones (in practice a threshold of 10^{-4} was adopted, corresponding to the accuracy of the overall strain measurement). The next wetting step then started. For the thin samples prepared in this work, a wetting step lasted ~2 h and ~11 h were required for completing the entire test.

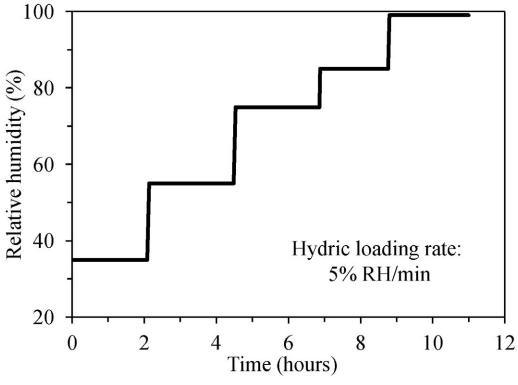

FIG. 2. Four-step wetting path of this work.

RESULTS

Plane 1

The four ROIs of plane 1 are shown in Figs 3–6 and their global principal strains are given in Fig. 7. These curves exhibit a bi-stage swelling: the strain is extremely small at low RH, while it becomes more significant at higher RH level. The threshold of this non-linearity is around 75%. Averaging the strains over the four ROIs, the major strain E_2 is 0.16% for the first stage from RH = 35% to 75%, and it becomes 0.93% for the second stage to 99% RH. One can refer to Wang (2012) for a detailed discussion on the mechanisms of this nonlinear swelling. The two principal strains are fairly similar in plane 1. The principal directions θ are dissimilar for the four studied zones. For instance, it is about 70º for zone 1, while it is 45º for zone 2 (see Fig. 13). All these results imply that there is no apparent global swelling anisotropy in plane 1. Indeed the fluctuations of principal directions Θ and the small differences between E_1 and E_2 are due to the small dimensions of the observation zones which are too small to be considered as representative volume elements (RVE). The measured average strains are thus sensitive to the local statistical realization of the microstructure.

The local strain fields (ε_2: major swelling strain) of the four ROIs in plane 1 are also presented (Figs 3–6). In general, the strain maps are very similar for different wetting steps. Hence, only the total strain maps (i.e. strain induced by 35–90% RH increase) are presented here and can be considered as representative of all wetting steps in terms of spatial distribution and local orientation of the strain field. The strain maps at such a local scale are strongly heterogeneous but well correlated to the microstructure: some violet and blue (i.e. low swelling) domains, naturally often located on the non-swelling inclusions, are wrapped by yellow and

https://doi.org/10.1180/claymin.2013.048.2.17 Published online by Cambridge University Press

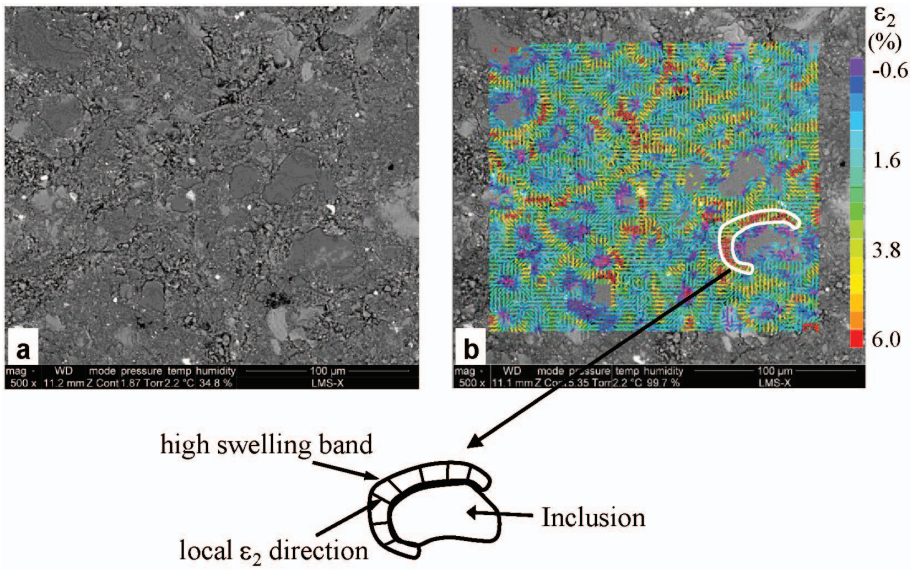

FIG. 3. Observation zone 1 of plane 1: (a) BSE image and (b) ε_2 strain map induced by a RH change from 35% to 99%. An example of a highly strained deformation band oriented along an inclusion boundary is outlined; moreover, the local ε_2 directions inside are perpendicular to its orientation, which implies that this band is associated with a swelling band.

red bands (i.e. high swelling) which are spread throughout the clay matrix. However there are also areas in the clay matrix which almost do not deform. In fact, this heterogeneous strain field results from a complex interaction phenomenon: the clay matrix tends to swell with increasing RH due to its specific swelling property, but it is inhibited by the non-swelling inclusions so that a local stress field would be generated even without external confinement. The heterogeneity inside the clay matrix, such as different clay groups with dissimilar swelling capacities and various clay particle orientations, may also contribute to the generation of local stresses. The total strain is indeed a sum of the free swellings and the strains induced by the internal stress field.

Concerning the high swelling bands in the clay matrix observed in plane 1, they are more or less randomly oriented, without any clear preferred orientation. In some cases, these swelling bands

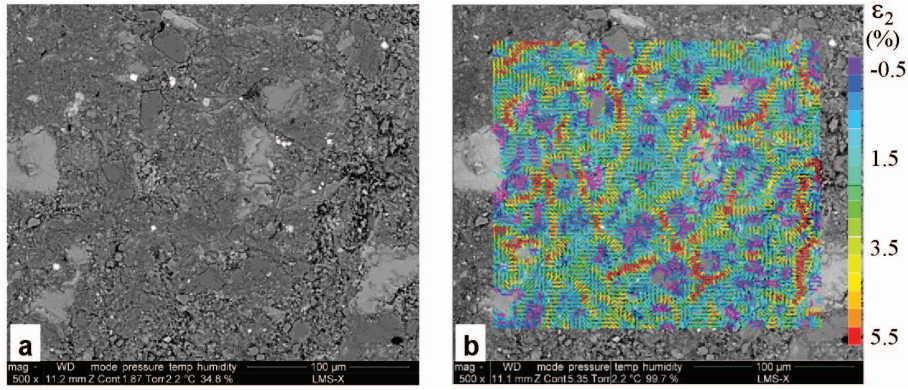

FIG. 4. Observation zone 2 of plane 1: (a) BSE image and (b) ε_2 strain map induced by a RH change from 35% to 99%.

https://doi.org/10.1180/claymin.2013.048.2.17 Published online by Cambridge University Press

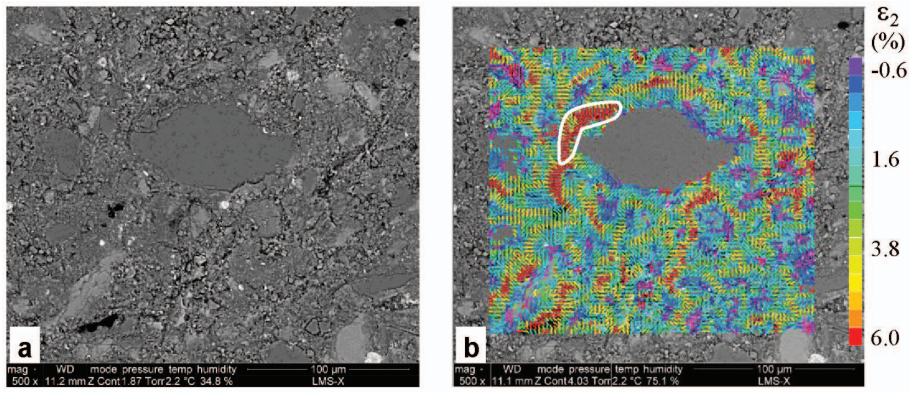

FIG. 5. Observation zone 3 of plane 1: (a) BSE image and (b) ε_2 strain map induced by a RH change from 35% to 99%. A micro-crack induced by wetting (i.e. decohesion of a coarse quartz grain from the clay matrix) results in a high strained domain, outlined in (b).

tend to drape the neighbouring inclusions so that their orientations are strongly controlled by the shape and orientation of the latter (an example is outlined in Fig. 3). The symbols used to represent local strains in strain maps are crosses with a major axis indicating the direction of major strain ε_2 (measured by local angle θ). It is shown that the local ε_2 directions are generally perpendicular to the local orientation of swelling bands (an illustration is given in Fig. 3). This implies that these deformation bands are indeed extension bands, rather than shear bands, for which the local ε_2 direction would be at 45° with respect to the orientation of the bands. The statistical distributions of these local principal directions θ in each ROI can be quantified by their probability distribution function (pdf) shown in Fig. 14. No preferred direction of local principal strain is observed in plane 1.

When the sample was humidified to extremely high RH (and only in that case), some micro-cracks appeared either in the clay matrix or on inclusion boundaries. The latter case is associated with decohesion of the inclusion-matrix interface which leads to a high local extension (an example is outlined in Fig. 5).

Plane 2

The four ROIs in plane 2 are shown in Figs 8–11. The bedding plane is horizontal in these images. Compared to plane 1, the inclusions in plane 2 are broadly smaller and seem to be more

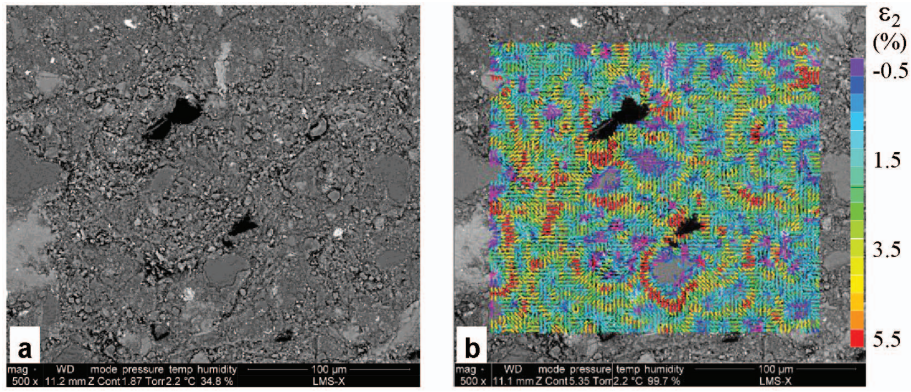

FIG. 6. Observation zone 4 of plane 1: (a) BSE image and (b) ε_2 strain map induced by a RH change from 35% to 99%.

https://doi.org/10.1180/claymin.2013.048.2.17 Published online by Cambridge University Press

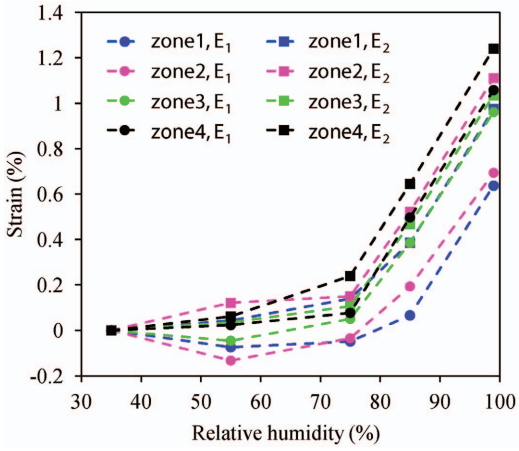

FIG. 7. Overall strains of the four observation zones in plane 1.

elongated. In addition, some pre-existing micro-cracks were found in all ROIs of plane 2, mostly extending along the bedding plane (i.e. horizontal in the image). This suggests a probable damage of the sample for plane 2 before the test, which was not observed in plane 1 even though samples were prepared under the same conditions. The overall strains of the four ROIs are presented in Fig. 12. Similar to plane 1, the bi-stage swelling is also evident on the strain curves, and the threshold seems to lie between 75% and 85% RH. However, in contrast to the swelling isotropy in plane 1, noticeable anisotropy is manifest in plane 2. The average major strain E_2 of the four ROIs is 1.12% for 35–99% RH change and E_1 is 0.32%, so the swelling anisotropy (ratio of E_2 to E_1) is 3.5. Moreover, in opposition to various values measured in plane 1, the principal directions Θ are always close to 0º for all the four observation zones in plane 2 (Fig. 13), indicating that the preferred swelling direction is perpendicular to the bedding plane, as already noticed by other authors (e.g. Pham et *al.*, 2007).

It should be noted that the major strain E_2 in plane 2 is comparable with the principal strains in plane 1, though the two samples with different observation planes were extracted from a same larger core sample. This is in disagreement with the existing macro-scale results (Valès, 2008), which have revealed that E_2 is much greater than E_1 in plane 2 and that the latter is comparable to the principal strains E_1 and E_2 measured in plane 1. In the present case, one would similarly expect the similar principal strains in plane 1 to be comparable

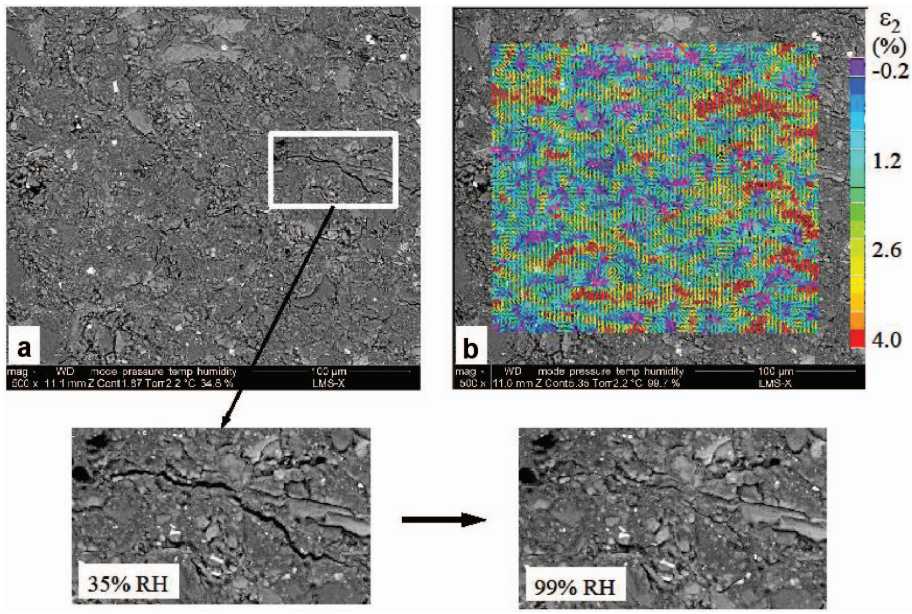

FIG. 8. Observation zone 1 of plane 2: (a) BSE image and (b) ε_2 strain map induced by a RH change from 35% to 99%. Closing of a pre-existing micro-crack during wetting is observed.

https://doi.org/10.1180/claymin.2013.048.2.17 Published online by Cambridge University Press

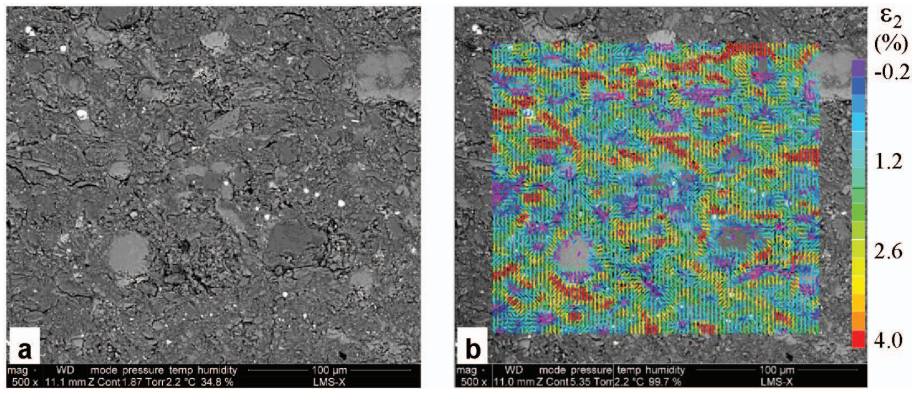

FIG. 9. Observation zone 2 of plane 2: (a) BSE image and (b) ε_2 strain map induced by a RH change from 35% to 99%.

to the minor strain parallel to the bedding plane in plane 2. The reason why this is not the case, more precisely why the strains in plane 1 are much larger for similar RH variations, is not clear. This might be related to the prior damage caused during sample preparation as suggested by the formation of cracks parallel to the bedding plane observed in plane 2 (as shown in Fig. 8) but not in plane 1. Under wetting, the swelling of the clay matrix is partly offset by closing of pre-existing micro-cracks so that the global E_2 would be much smaller than that on an undamaged sample. This could explain a low value of E_2 in plane 2, since these cracks are mostly parallel to the bedding plane, but hardly the high strain values in plane 1. Another possible cause could be a difference in mineral composition in ROIs, but no significant difference in inclusion content (from a rough estimation on BSE images) was observed between the two planes. A third explanation could be that the thin samples have undergone an additional overall bending because moisture infiltration would preferably proceed from the observation surface, and not from the opposite side. Swelling would be larger on the upper surface than on the lower one during the transient stages of the test. This may lead to an overall irreversible strain, still present when hydric equilibrium is reached. Such a bending would be bi-directional for plane 1 and unidirectional for plane 2, because of the anisotropy of the material. The detailed analysis of such phenomena is left for further investigations. They should however not modify the

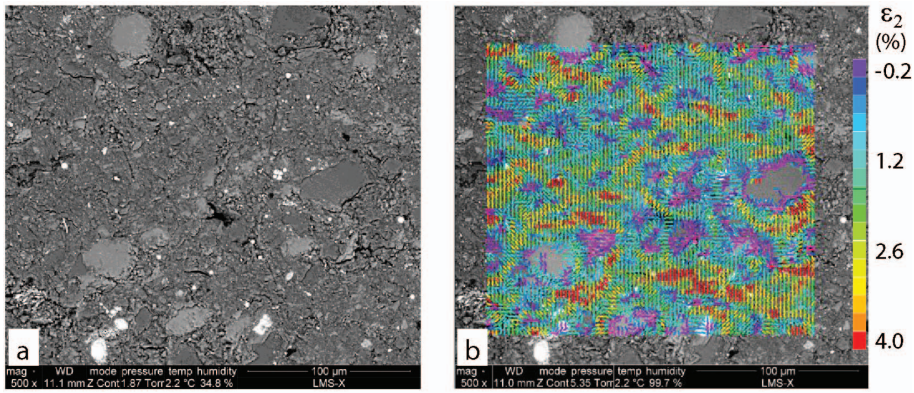

FIG. 10. Observation zone 3 of plane 2: (a) BSE image and (b) ε_2 strain map induced by a RH change from 35% to 99%.

https://doi.org/10.1180/claymin.2013.048.2.17 Published online by Cambridge University Press

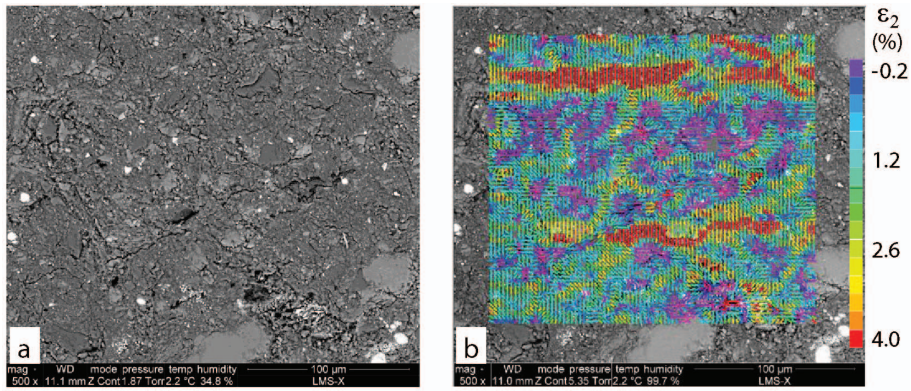

FIG. 11. Observation zone 4 of plane 2: (a) BSE image and (b) ε_2 strain map induced by a RH change from 35% to 99%.

directions of the local and global swellings which are under focus here.

The major swelling strain maps (again for 35−99% RH change) of the four ROIs in plane 2 are presented in Figs 8−11. Swelling bands are still observed but they are now preferentially oriented along the horizontal axis (i.e. parallel to the bedding plane). This is particularly true in zone 4 where two horizontal highly strained bands appear in the strain map (Fig. 11). This is clearly different from the observations in plane 1 in which no preferred orientation of swelling bands is observed. Moreover, the pdf of the local θ angle (Fig. 14) is concentrated between −30º and 30º and exhibits an intense peak at θ = 0º for all the four ROIs in plane 2. This means that the local ε_2 directions are predominantly normal to the bedding plane, which coincides with the global Θ.

In summary, there are clearly some features in the observations of planes 1 and 2 which are dissimilar. In plane 1, the overall strain is fairly isotropic, the high swelling bands are randomly oriented in strain maps, and so are the local ε_2 directions. However, anisotropy manifests in plane 2; the overall strain is clearly larger along the direction normal to the bedding plane, swelling bands in strain maps are preferably parallel to the bedding plane, and a clearly preferred direction normal to the bedding plane is found for the local major strain.

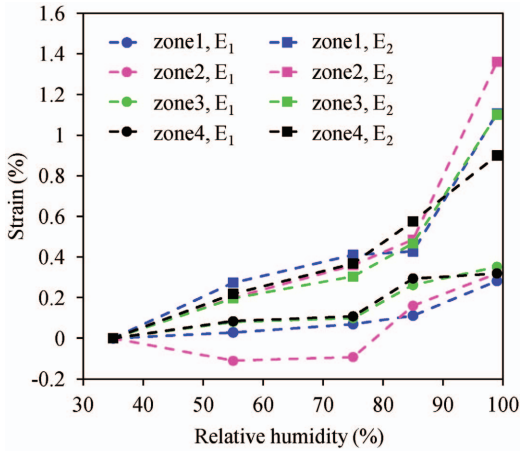

FIG. 12. Overall strains of the four observation zones in plane 2.

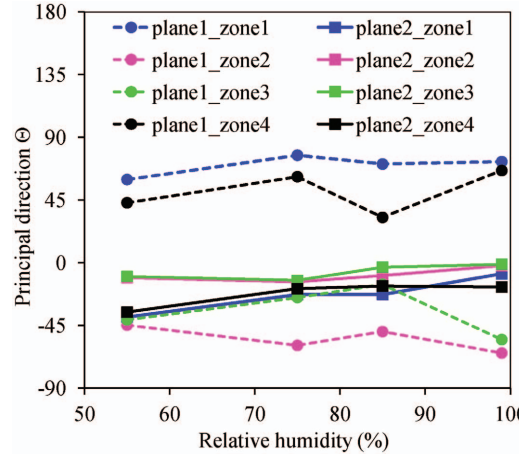

FIG. 13. Principal directions Θ of different zones in planes 1 and 2.

https://doi.org/10.1180/claymin.2013.048.2.17 Published online by Cambridge University Press

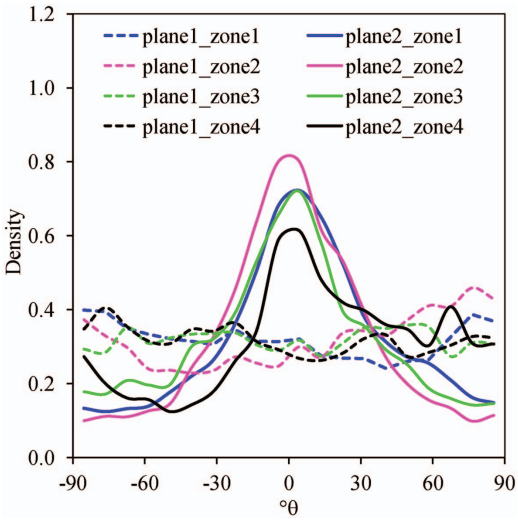

FIG. 14. Probability distribution function of θ in planes 1 and 2.

DISCUSSION

Preferred clay-particle orientation

The gauge length of the local strain measurements performed in this work is 5 μm, which is comparable to the size of a clay "aggregate" consisting of several individual micrometric clay particles with similar orientation. Hence, the ε_2 direction is likely to incorporate information about the clay-particle orientation; indeed the former would be normal to the latter under a free-swelling condition. However, as discussed previously, the strain measured here is a sum of the free swelling of clay minerals and the strain induced by the internal stress field. Because of the lamellar microstructure, the mechanical property of a clay particle is also strongly anisotropic with, in particular, a much larger deformability (i.e. lower stiffness) normal to the layers, so that the mechanical strain might also be predominant along this direction. Hence, the direction of the total strain may not deviate too much from the normal to the layers. As a consequence, the local ε_2 direction could be used, at least as a first approximation, as an indicator of the local clay-particle orientation. This interpretation is at least consistent with the observed distribution of local strain orientations (Fig. 14), with no preferred orientation in plane 1 and a pronounced alignment normal to the bedding plane in plane 2.

Another comment can be made on the orientation of deformation bands, which has been often been found to be normal to the local ε_2 direction. As a consequence, the orientation of these swelling bands is expected to be mostly aligned with the local clay particle layers. This would again be consistent with the fact that the deformation bands are mostly parallel to the bedding plane in observation plane 2, and more randomly distributed in plane 1. An additional mechanism of the preferred orientation of swelling bands is the spatial distribution of inclusions, which is essentially random in plane 1, but exhibits anisotropy in plane 2, consisting both in a preferred orientation of inclusions and in a tendency of grains to align with respect to each other along the bedding plane. These two phenomena may explain the global preferred orientation of deformation bands in plane 2 and its absence in plane 1. The detailed path of the deformation bands is, however, also determined by the complexity of the local mechanical interactions and the associated stress field induced by the incompatible swelling deformation of different constituents in the rock. Global expansion bands may thus locally be shear bands no longer parallel to clay particles. Hence, their orientation is less likely to be an indicator of the local particle orientation, in particular in the vicinity of inclusions where a considerable portion of the total strain is induced by mechanical stresses.

Anisotropic swelling of clay particles

From the arguments developed in the previous section, the local preferred orientation of clay particles could be estimated from the local ε_2 direction in this work. Another interesting question is to quantify the local swelling anisotropy of clay particles. As it is difficult to separate free-swelling strains from mechanical ones, a direct measurement of this quantity seems to be out of reach. However, it makes sense to quantify the total strain anisotropy on the scale of the clay particles. This is the purpose of this last section.

To do so, the pdf of the total local principal strains (35−99% RH) are quantified (Fig. 15). Local ε_1 strain pdf varies from −5% to 4% and exhibits a peak at 0 for both observation planes. The local ε_2 strain can attain 10% and the most frequent values are also comparable in the two planes; it is 2% for plane 1 and 1.5% for plane 2. In addition, the distribution function in plane 2 is

https://doi.org/10.1180/claymin.2013.048.2.17 Published online by Cambridge University Press

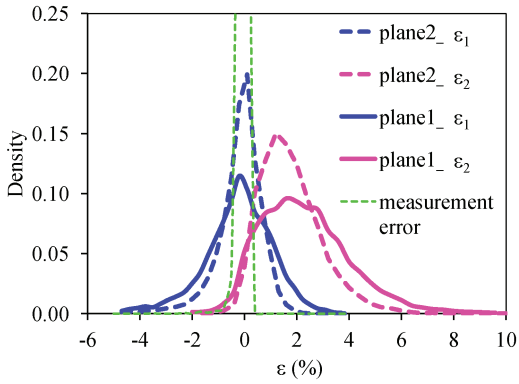

FIG. 15. Probability distribution function of principal strains in planes 1 and 2.

narrower than in plane 1, implying that the strain field in plane 2 is less heterogeneous.

Considering the measurement error (also shown in Fig. 15 and estimated by plotting the pdf of the principal strains obtained when comparing two images without deformation), the actual distributions of local ε_1 strains would be narrower (the presence of measurement errors tends to enlarge pdfs), so more concentrated around 0. This means that local swelling strains (of clay particles) are rather unidirectional. Hence, their anisotropy is very pronounced. One may evaluate from these data a lower limit of the local strain anisotropy from these pdfs. In plane 1, local ε_2 strain may reach 8% and more, while local ε_1 strain is almost always below 3%, so that the ratio between local principal strains is at least 2.7, which may explain the average anisotropy of 3.5 observed on the investigated ROIs on plane 2. This local anisotropy is much larger than the one observed at macroscopic scale which is of ~2 (Valès, 2008; Yang *et al.*, 2012).

Note also that the presence of negative local strains ε_1, which might sound surprising in a swelling experiment, can be explained by the complex mechanical interactions which can induce some compressive local strains.

In summary, among the various possible mechanisms of the swelling anisotropy, it seems that a strong local swelling anisotropy of clay particles, which are likely to deform almost unidirectionally, and a preferred orientation of these clay particles parallel to the bedding plane, is the most important one. The anisotropy of the shape, orientation and distribution of the other mineral inclusions is observed but is not pronounced. It may contribute to a faint preferred orientation of deformation bands parallel to the bedding plane but its contribution to the global swelling anisotropy seems to be limited.

CONCLUSION

By means of a combination of ESEM and DIC techniques, the swelling of COx argillaceous rock was investigated at the micrometric scale of its inclusion-matrix composite microstructure. The observations were conducted on two planes; parallel and perpendicular to the bedding plane. The physical size represented by a pixel in the images processed by DIC is about 60 nm, and the local strain gauge is 5 μm which is comparable to the size of clay particles.

Strongly heterogeneous local deformation fields induced by wetting were evident. They essentially result from the combination of the free swelling of the clay matrix and the mechanical strain associated with a local stress field induced by heterogeneity. The global swelling of this rock is known to be anisotropic, being more intense along the direction perpendicular to the bedding plane. Some anisotropy can be qualitatively discerned in the spatial distribution of the swelling bands observed in the clay matrix, which might be induced by anisotropic spatial distributions of clay and other mineral inclusions within the microstructure. But the proposed statistical analysis of local principal strains and of their directions strongly suggests that the main source of overall swelling anisotropy is related to the anisotropic clay particles and their orientation; they would undergo an almost unidirectional local swelling with increasing RH and exhibit a preferred orientation parallel to the bedding plane.

REFERENCES

Allais L., Bornert M., Bretheau T. & Caldemaison D. (1994) Experimental characterization of the local strain field in a heterogeneous elastoplastic material. *Acta Metallurgica et Materialia*, **42**, 3865–3880.

ANDRA (2005) Référentiel du Site Meuse/Haute-Marne: Vol. 2.

Bornert M., Orteu J.J. & Roux S. (2011) Corrélation d'images. Pp. 175–208 in: *Mesures de champs et identification en mécanique des solides* (M. Grédiac & F. Hild, editors). Hermès Science.

Ortega J.A., Ulm F.-J. & Abousleiman Y. (2007) The effect of the nanogranular nature of shale on their poroelastic behavior. *Acta Geotechnica*, **2**, 155–182.

Pham Q.T., Valès F., Malinsky L., Nguyen M.D. &

https://doi.org/10.1180/claymin.2013.048.2.17 Published online by Cambridge University Press

Gharbi H. (2007) Effects of desaturation-resaturation on mudstone. *Physics and Chemistry of the Earth*, **32**, 646–655.

Robinet J.C., Sardini P., Coelho D., Parneix J.C., Prêt D., Sammartino S., Boller E. & Altmann S. (2012) Effects of mineral distribution at mesoscopic scale on solute diffusion in a clay-rich rock: Example of the Callovo-Oxfordian mudstone (Bure, France). *Water Resources Research*, **48**, doi.org/10.1029/2011WR011352.

Sammartino S., Bouchet A., Prêt D., Parneix J.-C. & Tevissen E. (2003) Spatial distribution of porosity and minerals in clay rocks from the Callovo-Oxfordian formation (Meuse/Haute-Marne, Eastern France) implications on ionic species diffusion and rock sorption capability. *Applied Clay Science*, **23**, 157–166.

Sayers C.M. (1994) The elastic anisotropy of shales. *Journal of Geophysical Research*, **99**, 767–774.

Sutton M.A., Orteu J.-J. & Schreier H.W. (2009) *Image correlation for shape, motion and deformation measurements: basic concepts, theory and applications.* Springer.

Valès F. (2008) *Modes de déformation et d'endommagement de roches argileuses profondes sous sollicitations hydro-mécaniques*. PhD thesis, Ecole Polytechnique, Palaiseau, France.

Wang L.L. (2012) *Micromechanical experimental investigation and modelling of strain and damage of argillaceous rocks under combined hydraulic and mechanical loads*. PhD thesis, Ecole Polytechnique, Palaiseau, France.

Wenk H.R., Voltolini M., Mazurek M., Van Loon L.R. & Vinsot A. (2008) Preferred orientations and anisotropy in shales: Callovo-Oxfordian shale (France) and Opalinus Clay (Switzerland). *Clays and Clay Minerals*, **56**, 285–306.

Yang D.S., Bornert M., Chanchole S., Gharbi H., Valli P. & Gatmiri, B. (2012) Dependence of elastic properties of argillaceous rocks on moisture content investigated with optical full-field strain measurement techniques. *International Journal of Rock Mechanics & Mining Sciences*, **53**, 45–55.